



UvA-DARE (Digital Academic Repository)

Non-contact spectroscopic age determination of bloodstains

Bremmer, R.H.

Publication date
2011

[Link to publication](#)

Citation for published version (APA):

Bremmer, R. H. (2011). *Non-contact spectroscopic age determination of bloodstains*. [Thesis, fully internal, Universiteit van Amsterdam].

General rights

It is not permitted to download or to forward/distribute the text or part of it without the consent of the author(s) and/or copyright holder(s), other than for strictly personal, individual use, unless the work is under an open content license (like Creative Commons).

Disclaimer/Complaints regulations

If you believe that digital publication of certain material infringes any of your rights or (privacy) interests, please let the Library know, stating your reasons. In case of a legitimate complaint, the Library will make the material inaccessible and/or remove it from the website. Please Ask the Library: <https://uba.uva.nl/en/contact>, or a letter to: Library of the University of Amsterdam, Secretariat, P.O. Box 19185, 1000 GD Amsterdam, The Netherlands. You will be contacted as soon as possible.

We report on a non-contact method to quantitatively determine blood volume fractions in turbid media by reflectance spectroscopy in the VIS/NIR spectral wavelength range. This method will be used for spectral analysis of tissue with large absorption coefficients and assist in age determination of bruises and bloodstains. First, a phantom set was constructed to determine the effective photon path length as a function of μ_a and μ_s on phantoms with an albedo range: 0.02-0.99. Based on these measurements, an empirical model of the path length was established for phantoms with an albedo > 0.1 . Next, this model was validated on whole blood mimicking phantoms, to determine the blood volume fractions $\rho=0.12-0.84$ within the phantoms ($r=0.993$; error $< 10\%$). Finally, the model was proved applicable on cotton fabric phantoms.

CHAPTER 4
**NON-CONTACT SPECTROSCOPIC DETERMINATION OF LARGE BLOOD
VOLUME FRACTIONS IN TURBID MEDIA**

Biomedical Optics Express, Vol. 2, Issue 2, pp. 396-407 (2011)



INTRODUCTION

Optical measurements of biological media (e.g. whole blood or tissue) can be used to estimate physiological or morphological parameters of the sampled medium. Therefore, reflectance spectroscopy is a widely used technique to determine the optical properties of turbid media. Classical reflectance probe geometries involve contact between the probe and tissue. However, some applications in the forensic and clinical fields favor, or even require, no contact with the sample during measurement.

In forensic science, age determination of bloodstains can be crucial in reconstructing crime events. Upon blood exiting the body, hemoglobin saturates with oxygen in the ambient environment. Over time, the oxyhemoglobin auto-oxidizes into methemoglobin, and finally methemoglobin denaturates into hemichrome [23]. This oxidation cascade is typical for extracorporeal blood and the state of oxidation indicates the age of the bloodstain. Discrimination between these hemoglobin derivatives requires sampling in the wavelength range where these chromophores can be distinguished on the absorption properties, which is in the spectral range 450–650 nm. Despite several attempts [19, 35, 58], currently no reliable methods are available for determining the age of a bloodstain. In chapter 2, we showed that reflectance spectroscopy is a suitable candidate for age estimation, by determining the composition of various hemoglobin compounds in a bloodstain. Reflectance spectroscopy has the potential to detect the unique absorption bands of each of the heme-containing compounds, and potentially provide age-information about the bloodstains. In order to avoid contamination and cross-contamination and preserve the original crime scene [62], the measurement ideally must be made without contacting the sample.

Recent studies have shown the potential of non-contact reflectance spectroscopy for PDT monitoring [92, 93], monitoring apoptosis [94] and lung cancer detection [95]. These applications of spectroscopy do not require quantitative analysis of the reflectance spectra. Yu *et al* [96] and Saager *et al* [97] have shown a quantitative non-contact system, but their approaches require lenses, complicated scanning and only have small working distance, moreover not very applicable on crime scenes. In addition, those systems can only measure absorption coefficients up to 0.3 mm^{-1} , not high enough to measure the absorption coefficient of whole blood in the VIS/NIR spectral range. An alternative approach to non-contact spectroscopy is hyper-spectral imaging, but most spectral imaging systems are also only suitable in the low absorption regime [98].

Quantitative analysis of reflectance spectra is complicated because the path travelled by collected photons depends on the optical properties of the sampled medium. Yet by establishing a relation between the absorption and scattering properties of the sample and the photon path length, the chromophores and photon path length can be determined simultaneously. For measurements of extracorporeal blood, bruises [99] or other tissue containing large blood volume fractions, a reflectance spectrum in the visible, near-infrared wavelength region can cover an extreme range of absorption coefficients, $\mu_a = 0.1\text{-}30 \text{ mm}^{-1}$ [31]. Reflectance analysis techniques that are based on the diffusion

approximation [100] are not *a priori* applicable to these measurements as diffusion theory requires $\mu_s' \gg \mu_a$. Many more (semi-) empirical models have been reported in literature for quantitative analysis of reflectance spectroscopy measurements in contact mode [101-104]. Although these studies describe reflectance analysis methods, none has proven applicable on large absorption coefficients. However, recent studies have shown that quantitative analysis of reflectance spectra is achievable if the relationship between the photon path length and optical properties are well-defined [105-107].

This study presents a method for a quantitative determination of μ_a by analysis of non-contact reflectance measurements containing high absorption values. The difficulty and novelty of this work is combining non-contact, high absorption and quantitiveness. A quantitative method is required for required for measuring perfusion or blood volume fraction in a bruise, non-contact is required for avoiding contamination in case of a bloodstain; and high absorption is required considering the high absorption coefficients of whole blood in the visible part of the spectrum. This work investigates the sensitivity of the detected attenuation in the reflectance signal to the probe position and orientation to the measured sample. By mixing Intralipid 20%, a saline solution and Evans Blue, phantoms with a wide range of optical properties were constructed. Following the approach of Kanick *et al* [105, 106], we measured optical phantoms to construct an empirical model of the non-contact reflectance photon path length dependence on the absorption coefficient and reduced scattering coefficient of the optically sampled medium. The model of path length is utilized on whole blood mimicking phantoms for a spectral analysis algorithm to quantitatively determine chromophores concentrations. Finally the model is tested feasible for reflectance measurements on cotton fabric.

METHODS

Non-contact reflectance spectroscopy

The reflectance measurements were performed with a device composed of a spectrograph (USB 4000; Ocean Optics; Duiven, the Netherlands), a tungsten-halogen light source (HL-2000; Ocean Optics; Duiven, the Netherlands) and a non-contact probe (QR400-7-UV/BX; Ocean Optics; Duiven, the Netherlands). This probe contains six 400 μm core diameter delivery fibers, circularly placed around an identical central collection fiber. The core-to-core fiber distance is 450 μm , and the fiber has an NA of 0.22. The illumination spot size diameter is 6 mm, which realizes an overlap between illumination field and detection field. Figure 1 shows the schematic of the setup. The probe is positioned above the phantom, such that the probe angle α , and probe height h can be controlled. Only photons that have travelled through the phantom are considered useful, therefore specular reflection should be avoided. During measurements, photons emitted by the delivery fibers scatter through the phantom, and are collected with the central fiber. The light intensity measured with the collection fiber is the reflectance $R(\lambda)$, which is wavelength (λ) dependent. Attenuation

of R by the presence of chromophores can be described using an application of the Beer Lambert law, as follows:

$$R(\lambda) = R_0(\lambda) \exp[-\mu_a^i(\lambda) \cdot c_i \cdot \tau(\mu_s', \mu_a)] \quad (1)$$

In Eq. (1) R_0 is the reflectance of the phantom without the presence of absorbers. The specific absorption coefficient $\mu_a^i(\lambda)$ ($\text{l}\cdot\text{g}^{-1}\cdot\text{mm}^{-1}$) depends on wavelength, whereas c_i is the concentration of chromophore i ($\text{g}\cdot\text{l}^{-1}$). Finally, $\tau(\mu_s', \mu_a)$ is the effective path length (mm) of collected photons, which depends on μ_s' and μ_a of the phantom, and in turn, is wavelength-dependent.

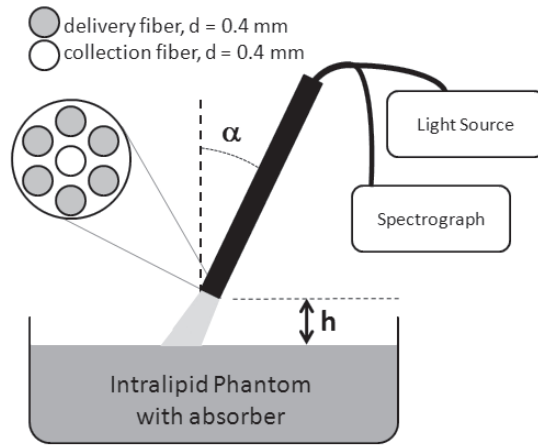


Figure. 1. Schematic of the non-contact reflection spectroscopy probe. The probe tip shows six delivery fibers, circulated around a central collection fiber. The delivery fiber is connected to the light source and the collection fibers are connected to the spectrograph.

Phantom preparation

This study involved three series of optical phantom experiments: 1) phantoms containing Evans Blue as an absorber; 2) phantoms containing hemoglobin for experimental validation of the analysis algorithm and 3) Evans Blue on cotton fabric.

For the first phantom series μ_a was controlled by varying the concentration of Evans Blue, which has a specific absorption maximum of $18 \text{ l}\cdot\text{g}^{-1}\cdot\text{mm}^{-1}$ at 611 nm. The μ_s' of each phantom was selected by varying the amount of Intralipid 20% (Fresenius Kabi AG, Bad Homburg, Germany), which has in undiluted form a reduced scattering coefficient, μ_s' of 18 mm^{-1} and an anisotropy of $g=0.75$ at 611 nm [108]. Estimations of reduced scattering coefficient for high Intralipid concentrations ($>8\%$) were corrected for dependent scattering effects[109]. Optical phantoms containing Evans Blue were constructed with absorption coefficients of $\mu_a = [0.1, 0.2, 0.4, 1, 2, 3, 5, 10, 20] \text{ mm}^{-1}$, at both $\mu_s' = 1 \text{ mm}^{-1}$ and at 11.5 mm^{-1} . Also a set was constructed with varying reduced scattering coefficients of $\mu_s' = [0.2, 0.5, 1, 2, 3.8, 5.5, 8.9, 11.5, 12.8, 13.6, 15.3] \text{ mm}^{-1}$,

at both $\mu_a=1 \text{ mm}^{-1}$ and at $\mu_a=10\text{mm}^{-1}$. The phantoms cover a range of albedo values, $A = \mu_s' / (\mu_s' + \mu_a) = [0.02-0.99]$. Additional phantoms were prepared at each selected μ_s' with no Evans Blue added, which were utilized to obtain baseline measurements of R_0 that represented $\mu_a=0 \text{ mm}^{-1}$ at 611 nm. For high reduced scattering, $\mu_s' > 2 \text{ mm}^{-1}$, each phantom was 40 mL and hold in cylindrical container with radius of 44 mm and height 7 mm. For low reduced scattering, $\mu_s' < 2 \text{ mm}^{-1}$, each phantom consisted of a 6-L sample hold within a 20-cm-edge cubed container. The large set of optical properties represents the wide range of absorption coefficients of bloodstains in the VIS/NIR wavelength region.

The second phantom series contained hemoglobin as the absorber. Aqueous hemoglobin was prepared by drawing human blood from a healthy, nonsmoking volunteer. The whole blood was washed by centrifuging the suspension at 2000 rpm, after which the supernatant was decanted. The remaining red blood cells (RBC) were resuspended with an amount of PBS equal to the decanted volume. This process was repeated twice. After the third time, when the supernatant was clear, the resuspension was performed with demineralized water for hemolysing the RBCs. The aqueous hemoglobin was removed from the suspension by centrifuging the suspension at 8000 rpm and decantation. In order to keep the amount of hemoglobin equivalent to the original blood volume fraction, the amount of resuspended liquid was kept equal to the amount of decanted liquid. The undiluted solution was assumed to have an amount of hemoglobin equivalent to a blood volume fraction, ρ , of 1; which corresponds to a hemoglobin concentration of 150 mg/ml and a molar concentration of 9.3 [mM] [110]. The phantoms were constructed with a range of absorption coefficients, equivalent to a blood volume fraction of $\rho = [0.84, 0.60, 0.47]$ for $\mu_s' = 3.5 \text{ mm}^{-1}$, $\rho = [0.75, 0.54, 0.42]$ for $\mu_s' = 6 \text{ mm}^{-1}$, $\rho = [0.50, 0.36, 0.28]$ for $\mu_s' = 10 \text{ mm}^{-1}$, and $\rho = [0.25, 0.18, 0.14]$ for $\mu_s' = 12 \text{ mm}^{-1}$. Additional phantoms were also prepared at each selected μ_s' with no hemoglobin added, to obtain baseline measurements of R_0 . The optical properties of the hemoglobin phantoms are chosen such that they fall with the range of optical properties of the Evans Blue phantoms. All Hb phantoms consisted of 40 mL and hold in cylindrical container with radius 44 mm and height 7 mm.

A third phantom series was made by pipetting aqueous Evans Blue onto white cotton fabric, creating stains with a diameter of 2.5 cm. After vaporization of the water, the reflectance of the white cotton fabric R_0 and the reflectance of the Evans Blue stain R were measured. We observed that the Evans Blue was distributed over a smaller area than the solvent. The absorption coefficient in the stain was estimated to be equal to absorption coefficient of aqueous Evans Blue, as measured by transmission spectroscopy, multiplied by the ratio of the areas of the stain without and with Evans Blue (see inset of figure 7 for a photograph of an Evans Blue stain on cotton). These areas were calculated by using a line gauge for measuring the radii of the stain without r_1 , and with Evans Blue r_2 . This introduces a potential error in estimation of the absorption coefficient; which will be addressed in the discussion section.

2.3 Analysis of photon path length

Eq (1) was used to describe the attenuation between spectra measured in phantoms with and without absorber present. The difference between the reflectance R , with absorber, and R_0 , without absorber, was attributed to the difference in absorption coefficient between the two samples. The reflectance was recorded at a resolution of 0.17 nm per pixel over a wavelength range of 450-900 nm. The data were smoothed by averaging data into bins of 10 pixels, which allowed the calculation of a standard deviation that represents noise within the signal. The effective photon path length for the Evans Blue phantom series was determined at 611 nm as shown in Eq. (2):

$$\tau_{611} = \frac{-\ln[R(611)/R_0(611)]}{\mu_a^i(611) \cdot c_i} \quad (2)$$

2.4 Empirical model of the photon path length

Based on observations of the effect of μ_a and μ_s' on the effective path length of the detected photons, and based on the photon path behavior for a single fiber geometry [105], the following empirical model for the effective path length was selected:

$$\tau_{\text{mod}}(\mu_s', \mu_a) = \frac{p_1(d \cdot \mu_s')^{p_2}}{p_3 + (d \cdot \mu_a)^{p_4}} \quad (3)$$

The empirical model Eq (3) has four fit parameters, two for the dependence on reduced scattering and two for the dependence on absorption. Here, the parameter set $[p_1, p_2, p_3, p_4]$ is fitted by minimizing the residual error between measured photon path length τ , and the predicted photon path length τ_{mod} . p_1 has units of mm, whereas p_2 - p_4 are dimensionless, finally d is a constant of unit length, set to be $d=1$ mm. The estimation of model parameters was achieved using a Levenberg-Marquardt fitting algorithm. The fit was weighted by the measured path length value at that point. The error margin on parameter estimation is represented by the 95% confidence intervals.

2.5 Spectral fit and determination of chromophore concentrations

Our observations on Evans Blue as absorber are employed for the phantoms with hemoglobin, which is more realistic for forensic applications. The attenuation of the reflectance signal with respect to the reflectance without absorber is the product of the absorption coefficient and the modeled photon path length. The total absorption is the sum of the three hemoglobin derivatives possible present in the phantom:

$$\mu_a = x_1 \cdot \mu_a^{\text{Hb}} + x_2 \cdot \mu_a^{\text{HbO}_2} + x_3 \cdot \mu_a^{\text{met-Hb}} \quad (4)$$

Knowledge of the absorption coefficients of deoxygenated, oxygenated, and met-hemoglobin for a large spectral range [31] enables a spectral fit. The spectral fit processes three fitted parameters. $[x_1, x_2, x_3]$ were obtained by reducing the weighted sum squared error between measured and model estimated reflectance. x_1 is the concentration of deoxygenated hemoglobin, x_2 is the concentration of oxygenated

hemoglobin, and x_3 is the concentration of met-hemoglobin. The total absorption μ_a is implemented in the empirical path length model, while the modeled effective path length τ is adjusted simultaneously as a function of the total absorption, according to Eq. (3). The total blood volume fraction is given as the sum of x_1 , x_2 and x_3 ; finally the oxygen saturation is given as: $x_2/(x_1 + x_2)$. The empirical model has an additional fit factor x_4 to correct mismatches in reflectance amplitude; typically these mismatches were less than 5%. Summarizing, the spectral fit for reflectance ratio of the empirical model is a combination of Eq. (3) and Eq. (4):

$$\frac{R(\lambda)}{R_0(\lambda)} = x_4 \exp\{-\mu_a \cdot \tau_{\text{mod}}\} \quad (5)$$

Eq. (5) has four fit parameters: $[x_1, x_2, x_3, x_4]$. Parameter estimation was achieved using a Levenberg-Marquardt algorithm that was scripted into LabView code (National Instruments); which allows for real-time fit parameter estimation. This model accounts for wavelength dependent scattering as an input into τ . In this study, μ_s' estimation was performed by relating it to the concentration of Intralipid as by Van Staveren [108].

RESULTS

3.1 Reflectance data

Figure 2 shows the reflectance ratio of an optical phantom of Intralipid with Evans Blue, R ($\mu_a=2.5 \text{ mm}^{-1}$ and $\mu_s' = 11.5 \text{ mm}^{-1}$) and a phantom of Intralipid without Evans blue R_0 ($\mu_a=0 \text{ mm}^{-1}$ and $\mu_s' = 11.5 \text{ mm}^{-1}$). At $\lambda=611 \text{ nm}$, Evans Blue has its absorption maximum, which is shown by the minimum in the reflectance ratio. At longer wavelengths, $\lambda>750 \text{ nm}$, Evans Blue does not absorb, so the reflectance ratio approaches 1. The effective photon path, τ of the collected photons with $\lambda=611 \text{ nm}$ from the measurement of Intralipid and Evans Blue can be calculated with Eq 2; here $\tau = 0.61 \text{ mm}$.

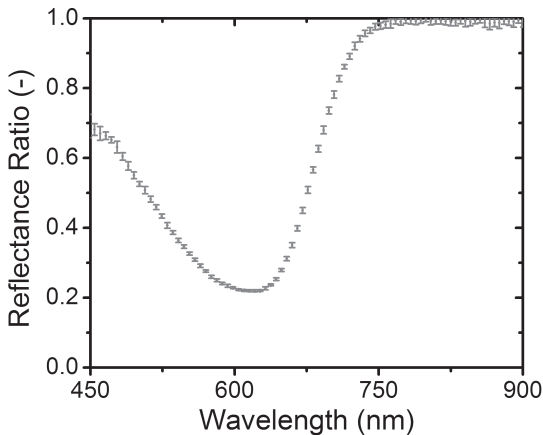


Figure 2. Reflectance ratio of phantom containing Evans Blue + IL and Intralipid without absorber. Only the reflectance ratio at $\lambda=611 \text{ nm}$ is used of the path length analysis. Here at $\lambda=611 \text{ nm}$, $\mu_a=2.5 \text{ mm}^{-1}$ and $\mu_s' = 11.5 \text{ mm}^{-1}$. The error margin represents SD.

By adjusting the height and the angle of the probe, the dependency of the effective photon path on the probe position could be determined. We found that for probe heights $h > 15$ mm, the variations in effective photon path length are below 3%. Also for $\alpha > 10^\circ$ the effective photon path length becomes insensitive for changes of probe angle, variations in effective photon path length on probe angle are below 2% for $\alpha > 10^\circ$. Based on these observations we use a probe geometry with a height $h = 17$ mm and an angle $\alpha = 13^\circ$ for the rest of the experiments.

3.2 Path length dependence on μ_a and μ_s'

Figure 3 shows the effective photon path length versus μ_a at high reduced scattering, $\mu_s' = 11.5 \text{ mm}^{-1}$, and at low reduced scattering, $\mu_s' = 1 \text{ mm}^{-1}$. The figure shows that the effective photon path length decreases for increasing absorption coefficient, both for high and low reduced scattering coefficient; an expected result as photons with longer path lengths are more likely to be absorbed, and therefore, less likely to be detected, resulting in the reduction of the path length. Figure 4 shows the effective photon path length versus μ_s' at high absorption, $\mu_a = 10 \text{ mm}^{-1}$, and at low absorption, $\mu_a = 1 \text{ mm}^{-1}$. At low absorption, the effective photon path length decreases for increasing reduced scattering. The effective photon path length is almost insensitive for changes in reduced scattering at high absorption. In both figure 3 and 4 the empirical path length model at our region of interest is plotted as a solid line.

The smallest residual error between measured data and model predictions resulted in the following estimated parameter values: $p_1 = 2.73 \pm 0.33 \text{ mm}$, $p_2 = -0.32 \pm 0.03$, $p_3 = 0.22 \pm 0.11$, $p_4 = 0.68 \pm 0.06$. The empirical model shows good agreement with the measured data, as showed by the Pearson correlation coefficient: $r^2 = 0.997$. The empirical model holds over a wide range of optical properties and photon path lengths (range: 0.15 – 6.4 mm). However, attempts to construct a model for the total set were not successful. Therefore we had to excluding data points with albedo < 0.1 . The excluded regions of the model are plotted with a dashed line in figures 3 and 4.

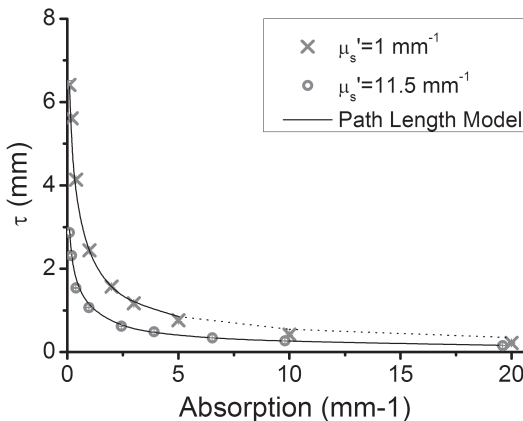


Figure 3. Effective photon path length vs absorption, the absorption coefficients was varied from $\mu_a = 0.1$ - 20 mm^{-1} ; measured at a reduced scattering coefficient of $\mu_s' = 1 \text{ mm}^{-1}$ (crosses) and $\mu_s' = 11.5 \text{ mm}^{-1}$ (open circles). The black line shows the path length model; dotted black line show model predictions for excluded data points.

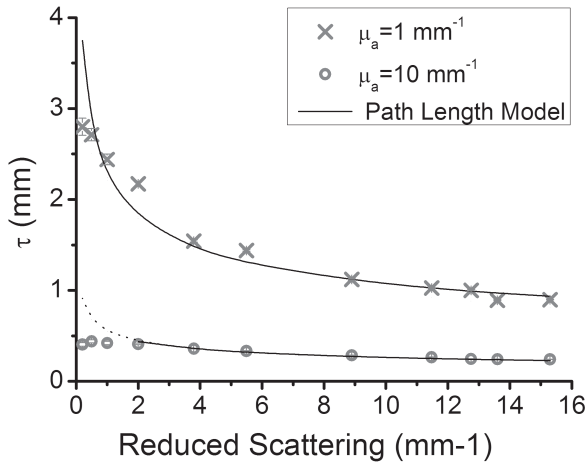


Figure 4. Effective photon path length vs reduced scattering. The reduced scattering coefficient varies from $\mu'_s = 0.2$ - 15.3 mm^{-1} . Measured at an absorption coefficient of $\mu_a = 1 \text{ mm}^{-1}$ (crosses) and $\mu_a = 10 \text{ mm}^{-1}$ (open circles). The solid line shows the path length model; dotted black line shows model predictions for excluded data points.

3.3 Hemoglobin Phantoms

Figure 5 shows the reflectance ratio of an optical phantom of Intralipid 10% with and without hemoglobin, for the spectral range of 450-900 nm. The gray dots represent the measured reflectance ratio, and the solid line is a spectral fit to model the reflectance measurement. The attenuation of the reflectance signal with respect to the reflectance without absorber is the product of the absorption coefficient and the modeled photon path, (Eq 3) with the parameter values as presented in section 3.2. The squared Pearson product correlation coefficient for the spectral fit is: $r^2=0.999$. The determined effective photon path through the phantom is shown on the right vertical axis. At $\lambda=576 \text{ nm}$, at the absorption maximum of HbO_2 , the effective photon path is 0.5 mm , whereas at $\lambda=675 \text{ nm}$, at which HbO_2 has an absorption minimum, light penetrates the optical phantom much deeper, accordingly $\tau = 4 \text{ mm}$.

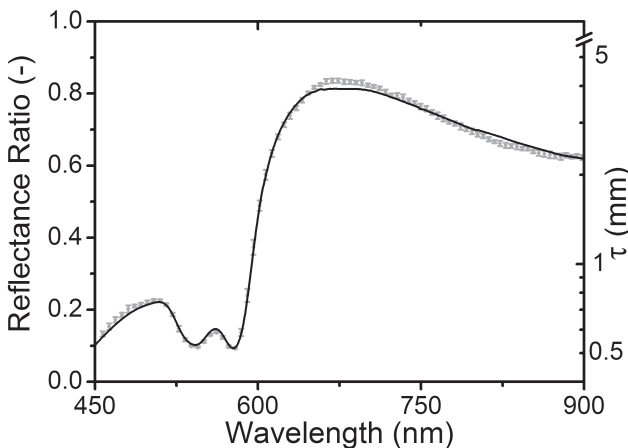


Figure 5. Typical reflectance measurements of an optical phantom containing of $\mu'_s = 10 \text{ mm}^{-1}$ at $\lambda=611 \text{ nm}$. The measured ratio is the ratio of the reflectance of an optical phantom with and without hemoglobin as absorber. Solid line is the spectral fit of the reflectance with HbO_2 ; $\rho=0.28$. The right hand axis shows the corresponding effective photon path through the phantom.

Figure 6 plots the measured blood volume fraction versus the experimental blood volume fraction. Model predictions were significantly correlated with measured values, as evidenced by a squared Pearson product correlation coefficient of $r^2 = 0.993$; this effect is observable in the plot as the data are scattered about the line of unity. The model holds for a wide range of blood volume fractions (range: 0.12-0.84) and absorption coefficients (range: 0.01-24 mm^{-1}), all with an albedo > 0.1 . The difference between input BVF and estimated BVF was less than 10% for all measurements. Model estimates of oxygen saturation, $x_2/(x_2+x_1)$ in Eq. (5), were determined to be close to fully oxygenated for all measurements: $99.6 \pm 0.9\%$ and no formation of methemoglobin was observed.

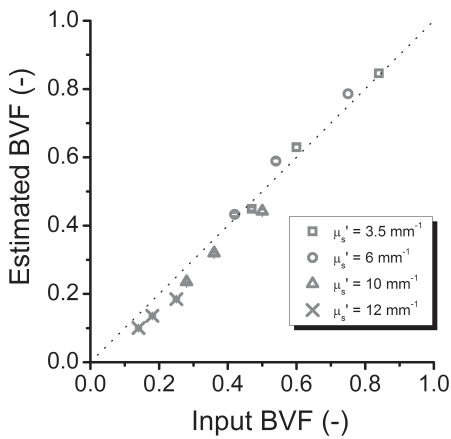


Figure 6. Optically estimated BVF, based on the spectral fits plotted against input BVF based on the phantom preparation for all twelve Hb phantoms at various reduced scattering coefficients.

3.4 Evans Blue on cotton

The effective photon path length as a function of absorption coefficient exhibits the same trend on cotton as in Intralipid: for increasing absorption, the photon path length decreases, which is shown in figure 7. The inset of figure 7 shows the radii of the stain, without and with Evans Blue, which is discussed at the end of the methods section. Determination of these radii and estimation of the absorption coefficient in the center of the stain introduces a potential error, which is depicted by the (horizontal) error bars in absorption coefficients. The effective photon path length is fitted by performing a non-linear least squares fit on Eq. (3) with only the reduced scattering coefficient of the cotton as fit parameter; other model parameters are based on the Intralipid measurements as presented in section 3.2. The fit is weighted by the inverse of the measurement error. We found: $\mu_s' = 53 \pm 31 \text{ mm}^{-1}$; here the error margins represent the 95% confidence interval of the fit. The origin of the large error margin will be addressed in the discussion.

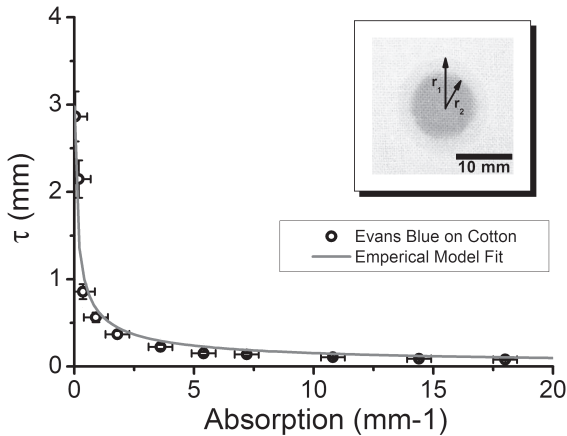


Figure 7. Effective photon path length vs absorption in white cotton fabric. The dots show the measured effective photon path length through Evans Blue and cotton. The blue line is the fit of the empirical path length. The inset is a photograph of the Evans blue on cotton showing the inner and outer radius of the stain, with and without Evans Blue.

DISCUSSION AND CONCLUSION

This study presents an analysis method that provides quantitative determination of μ_a for a non-contact reflectance spectroscopy device. Varying probe height and angle led to selection of probe setup that enables repeatable measurements, insensitive to small changes in height and angle. Observations of the dependency of the effective photon path length on the optical parameters of the tissue allowed implementation of an empirical model. The model gives a relation between μ_a and μ_s' of the phantom and the measured effective photon path length. Furthermore, the empirical model allows multi-component fit analysis of the reflectance spectra which enables quantitative chromophore determination. Conformation was found for the hemoglobin phantoms with a blood volume fraction of $\rho = [0.14-0.84]$. To the best of the authors' knowledge, this is the first time a non-contact device could quantitatively measure blood volumes over this wide range of optical properties and with μ_a up to 25 mm^{-1} .

Baseline measurements in this study were recorded using phantoms without the presence of absorbers. The baseline measurements account for the spectrum of the lamp, fiber through put, and need to be performed in similar probe configuration (height and angle) as the actual reflectance measurement. For application of measuring the reflectance of a bloodstain, baseline reflectance can be obtained by measuring the non-absorbing host matrix, such as cloth or paper. Similarly, reflectance measurements on bruises [99] can be performed in a kindred way when baseline measurements are taken on healthy skin, where absorption is more than ten times lower than in a bruise.

The effective photon path length for variations in absorption and reduced scattering coefficient had to be determined. A distinct trend was observed: τ decreases for increasing μ_a , however for μ_s' the observed trend is less definite (figure 4). At low absorption ($\mu_a = 1 \text{ mm}^{-1}$), τ decreases for increasing μ_s' , but at high absorption ($\mu_a = 10 \text{ mm}^{-1}$), τ is less sensitive to changes in μ_s' and does not follow a clear pattern especially in the low μ_s' region. This complicates the description of effective photon path length dependence on μ_a and μ_s' for low albedo values. Therefore, phantoms with albedo values

smaller than 0.1 were excluded and this model was selected based on the remaining data points. For most clinical and forensic application, the combination of high absorption and low scattering is not very relevant. Since *in vivo* the blood volume fraction does not exceed $\rho=0.2$, accordingly the absorption will be less than 6 mm^{-1} . However for bloodstains, higher absorption coefficients are present. Therefore, this approach is limited to bloodstains on host materials with high scattering coefficients, like paper or cotton. When the bloodstain has dried, the scattering of the bloodstain on cotton will be similar to the scattering of the cotton. In figure 4, the empirical model predictions deviate from the measurements for albedo < 0.1 , shown by dashed lines. Therefore, this model cannot be used in for on samples with an albedo < 0.1 . The developed relation for the effective photon path length is based on a single anisotropy value of $g=0.75$. Whole blood is known to have much higher anisotropy, $g>0.99$ [111]. Studies of other reflectance devices have shown that varying the anisotropy to higher g -values, while keeping μ_s' constant, did not influence the effective photon path length [105].

A typical reflectance measurement with corresponding spectral fit of a hemoglobin phantom is shown in figure 5. This spectral fit enables determination of the hemoglobin compounds, resulting in estimation of oxygen saturation and blood volume fraction. The spectral fit has a very high correlation with the measured reflectance and a nearly flat residue. The latter is required to ensure that the model is correct [75]. Because of the high affinity of hemoglobin for oxygen and the presence of oxygen in the atmosphere the hemoglobin will saturate totally as soon as it comes in contact with air. Hence the oxygen saturation in the hemoglobin phantoms was found nearly to be 100% for all measurements. No presence of met-hemoglobin was measured in the phantom, since all measurements were performed within an hour after phantom construction, which is too short for occurrence of autoxidation to methemoglobin. Figure 6 shows the determined BVF for the range of $\rho=0.14-0.84$. The spectrally determined BVF differs less than 10% from the true BVF for all measurements. The good agreement in combination with the expected high oxygen saturation indicates that all fitted parameters are correct and that quantitative determination of hemoglobin chromophores is possible.

The measurements with Evans Blue on cotton show that the cotton has a high reduced scattering coefficient at 611 nm: $\mu_s' > 20 \text{ mm}^{-1}$. We assumed that the scattering of the dried Evans Blue stain is similar to the reduced scattering of the cotton fabric without Evans Blue. The large error margin of the determined reduced scattering coefficient of cotton fabric is because the effective photon path is almost insensitive for changes in μ_s' for high values of μ_s' . This insensitiveness of μ_s' is also shown in figure 4, where it shows that the trend of effective photon path as a function of reduced scattering coefficient becomes almost flat for $\mu_s' > 10 \text{ mm}^{-1}$. We have assumed homogenous stains on cotton. This method will be applicable on bloodstains if the scattering of a bloodstain on cotton is similar as the scattering of clean cotton. Implementation on multi-layered structures, as bruises, which have a low absorbing layer (skin) on top of high absorbing layer (blood pool) will require validation on multi-layered phantoms [112].

In forensic science, these spectroscopic measurements will assist in detection and identification of traces at the crime scene [62]. The result of this study enables

analysis of bloodstain towards reconstruction of the time of crime, since determination of hemoglobin compounds in bloodstains or bruises allows estimation of the age of a bloodstain or bruise [99]. Especially for *on-site* bloodstain analysis, non-contact measurements are required to avoid trace contamination. To keep consistent optical coupling for bloodstain and baseline measurements a fixed probe is preferred. Bloodstains deposited on a non-white substrate would require a more sophisticated optical sampling and analysis method. For application in forensic practice the influence of background color has to be evaluated in a future study. Equally important are benefits for medical applications: non-contact measurements avoid pressure between skin and probe and therefore allow more reliable oxygen saturation measurements [113].

To conclude, the results presented in this study show that a simple non-contact spectroscopy device with a light source, fiber probe and spectrograph enables quantitative chromophore determination in the VIS/NIR wavelength range in homogeneous media. Furthermore we showed that these measurements can be used for forensic application as bloodstains on cotton fabric. This result expands the oxygen saturation measurements to fields with application specific requirements: no pressure and without blocking treatment light. Even more important, it allows implementation of reflectance spectroscopy in a forensic setting: on a crime scene.